

Robust superconducting correlation against intersite interactions in the extended two-leg Hubbard ladder

Zongsheng Zhou^{1,2,3}, Weinan Ye^{1,3}, Hong-Gang Luo^{1,3,4}, Jize Zhao^{1,3,*}, and Jun Chang^{5,†}


¹*School of Physical Science and Technology & Key Laboratory of Quantum Theory and Applications of MoE, Lanzhou University, Lanzhou 730000, China.*

²*Beijing National Laboratory for Condensed Matter Physics and Institute of Physics, Chinese Academy of Sciences, Beijing 100190, China*

³*Lanzhou Center for Theoretical Physics, Key Laboratory of Theoretical Physics of Gansu Province, Lanzhou University, Lanzhou 730000, China.*

⁴*Beijing Computational Science Research Center, Beijing 100084, China*

⁵*College of Physics and Information Technology, Shanxi Normal University, Xi'an 710119, China*

 (Received 27 June 2023; revised 31 October 2023; accepted 2 November 2023; published 17 November 2023)

The Hubbard and related models serve as a fundamental starting point in understanding the novel experimental phenomena in correlated electron materials, such as superconductivity, Mott insulator, magnetism. Recent numerical simulations demonstrate that the next-nearest-neighbor hopping t' plays a key role for the superconductivity. However, the impacts of long-range intersite interactions in such a t' -Hubbard model are less explored. Using the state-of-art density-matrix renormalization group method, we investigate the t' -Hubbard model on a two-leg ladder with the intersite interactions extended to the fourth neighbors. The numerical results show that the quasi-long-range superconducting correlation remains stable under the repulsive intersite interactions and these long-range repulsive interactions only change the ground state quantitatively. In addition, inspired by recent experiments on one-dimensional cuprate chain $\text{Ba}_{2-x}\text{Sr}_x\text{CuO}_{3+\delta}$, we find that the nearest-neighbor attractive interaction significantly enhances the superconducting correlation when it is comparable to the nearest-neighbor hopping t . Stronger attraction drives the system into an electron-hole phase separation. Finally, we discuss the effects of the on-site interaction on superconductivity.

DOI: [10.1103/PhysRevB.108.195136](https://doi.org/10.1103/PhysRevB.108.195136)

I. INTRODUCTION

Despite the extensive investigations in the last decades, the microscopic mechanism of high- T_c superconductivity in cuprates remains one of the challenging puzzles in condensed matter physics [1,2]. Single-band Hubbard model [3] and t - J model [4] are the simplest models frequently employed to understand experimental results in the high- T_c cuprates. The latter is the strong interaction limit of the former under hole doping, and it is also the low-energy effective model of the original three-band d - p model [5], which directly depicts the physics on the CuO_2 plane in high- T_c cuprates. In the single-band Hubbard model on a square lattice, many phases observed in high- T_c cuprates are reproduced, such as the antiferromagnetism at half-filling [6–8], the antiferromagnetic correlation upon hole doping [9], pseudogap [9–12], the stripe phase where charge density wave (CDW) and spin density wave (SDW) coexist around 1/8 doping [13,14], and metal phase in the overdoped regime [15]. This means that the Hubbard model does capture some ingredients of the high- T_c cuprates.

However, in the simplest Hubbard model current powerful numerical methods demonstrated that the ground state is not the superconducting state [14,16], but a stripe phase with

the wavelength of charge density $\lambda_c = 8$, which is recently observed in the experiment [17]. Meanwhile, numerical results indicate that the superconducting state is a high-energy excited state, and several stripe phases are highly competitive near the ground state [13,16,18–21]. These results imply that some crucial ingredients leading to superconductivity are missing in the simplest Hubbard model. Some other terms, such as the hopping term beyond the nearest-neighbor (NN) and the intersite interactions should be taken into account. Indeed, the next-nearest-neighbor (NNN) hopping t' brings impressive changes into the ground state. It not only chooses the wavelength of $\lambda_c = 4$ stripe state as the ground state [22] that is widely observed in experiments [23–25], but also induces quasi-long-range superconducting correlation on a four-leg cylinder [26–28]. Very recently, numerical simulations indicate that the t' -Hubbard model is adaptable in qualitatively capturing the physics in high- T_c cuprates [29]. Additionally, in actual materials, particularly in one and two dimensions, the Coulomb screening is relatively weaker than that in three dimensions. It is probably hard to screen the long-range interactions completely, and thus intersite interactions are still considerable [30,31].

Undoubtedly, it will be very difficult to numerically simulate the doped extended Hubbard model in the two-dimensional limit. As there are cuprate ladder superconducting materials [32–34], a deep understanding on these superconducting ladders can aid in comprehending the physics of two-dimensional cuprate materials due to their chemical

*zhaojz@lzu.edu.cn

†junchang@snnu.edu.cn

similarity. Actually, the Hubbard-related models on chains and ladders have been extensively studied [35–46] in the past decades. But the effect of the long-range intersite interaction on the t' -Hubbard model are less touched. In this work, we consider repulsive intersite interactions in the t' -Hubbard model as they originate from the Coulomb interaction. The situation may be different when there exists an electron-phonon coupling. For example, it was found recently that the Hubbard model with an attractive NN interaction, which may arise from electron-phonon coupling, could well explain the results of angle-resolved photoemission spectroscopy on the one-dimensional cuprate chain compound $\text{Ba}_{2-x}\text{Sr}_x\text{CuO}_{3+\delta}$ [47]. And recent numerical simulation on the Holstein-Hubbard chain indicates that an effective NN attraction can be mediated by long-range electron-phonon coupling [48]. Thus, it is also worthwhile exploring the t' -Hubbard model with attractive NN interaction. Here, focusing on a two-leg ladder and employing the density-matrix renormalization group (DMRG) [49–52] method, we investigate the effects of intersite interaction on the superconductivity in t' -Hubbard model. In particular, in the repulsive case the interaction is up to the fourth neighbor. Our numerical results indicate the superconducting correlation is slightly weakened but still robust under the repulsive intersite interactions. The charge density distribution, density correlation, and spin correlations are nearly undisturbed under the long-range repulsive intersite interactions. In sharp contrast to the repulsive interactions, the attractive NN interaction significantly strengthens the superconducting correlation when the attraction is comparable with the NN hopping t . The spin and density correlations show a nonmonotonic dependence on the attractive interaction. Prior to being driven into the electron-hole phase separation (PS), the ground state is the Luther-Emery (LE) liquid [53]. In addition, analyzing the different components of pairing correlation, we find that the pairing symmetry tends to be d wave. At last, we study the impacts of on-site interaction. Our numerical results show that very strong on-site interaction weakens the superconducting correlation under both the attractive and repulsive NN interactions. These results will be shown in detail in the later sections.

The content of the paper is organized as follows. Section II involves a brief introduction of the model and some details of DMRG simulations. In Sec. III, we investigate the effects of repulsive and attractive NN interactions on the t' -Hubbard model. In Sec. IV, we probe the long-range repulsive interactions up to the fourth neighbors. In Sec. V, with the presence of NN repulsive and attractive interaction, we explore how the ground state is affected by different on-site interaction U . This paper is closed by a summary in Sec. VI.

II. MODEL AND METHOD

The extended t' -Hubbard model on a two-leg ladder is written as

$$\mathcal{H} = -t \sum_{\langle ij \rangle \sigma} (c_{i\sigma}^\dagger c_{j\sigma} + \text{H.c.}) - t' \sum_{\langle\langle ij \rangle\rangle \sigma} (c_{i\sigma}^\dagger c_{j\sigma} + \text{H.c.}) + U \sum_i n_{i\uparrow} n_{i\downarrow} + \sum_{i \neq j} V_{ij} (n_{i\uparrow} + n_{i\downarrow})(n_{j\uparrow} + n_{j\downarrow}), \quad (1)$$

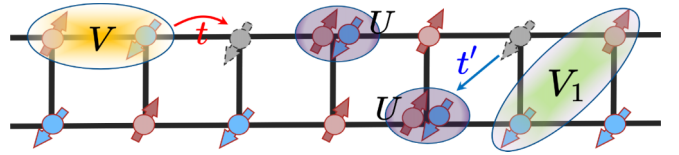


FIG. 1. A sketch diagram of the extended t' -Hubbard model on a two-leg ladder. t and t' represent the nearest- and the next-nearest-neighbor hopping, respectively. U is on-site repulsion. V and V_1 are the NN and the NNN intersite interactions. Intersite interactions beyond NNN are not shown here.

where the first and second terms in Eq. (1) represent the hopping terms between NN and NNN lattice sites, respectively. $c_{i\sigma}^\dagger$ ($c_{i\sigma}$) creates (annihilates) an electron at site i with spin σ . The third term is on-site repulsion for two electrons with different spins, in which $n_{i\sigma}$ is the number of electrons with spin σ . The last term describes the interaction among electrons at different sites. We assume the values of V_{ij} only depend on the distance between site i and j . To be visually intuitive, we illustrate the model Eq. (1) in Fig. 1.

In this work, we simulate the model Eq. (1) by utilizing the DMRG method, which has been shown as the most powerful method to study one- or quasi-one-dimensional systems. In numerical calculations, we set the NN hopping amplitude $t = 1$ as the energy unit, the NNN hopping amplitude $t' = -0.25$, and the on-site interaction $U = 8$ unless stated explicitly otherwise. These values are frequently used in related numerical simulations of high- T_c cuprates. The numbers of electrons with spin-up and spin-down in Eq. (1) are conserved, respectively. Thus, in the calculations the two $U(1)$ symmetries are implemented to lower the numerical costs. We retain up to $m = 8000$ states, and the largest truncation error is of the order of 10^{-7} . At least 20 sweeps are performed to ensure the calculations are well converged. The convergence of our DMRG results is also checked by the ground-state energy, expectation values of observations, and the von Neumann entropy. Our DMRG code is based on the ITensor library [54].

We adopt open boundary conditions in all the calculations. The system has $N = 2 \times L$ sites, and the largest system size we simulated reaches $L = 96$. Strong on-site interaction U freezes the charge degree of freedom at half-filling, and the ground state is a Mott insulator. Hole doping makes the magnetic order in the insulator unstable and drives the system into unconventional phases, probably including superconductivity. The filling factor is defined as N_e/N , where N_e is the electron number. The concentration of hole is $\delta = 1 - N_e/N$. Here, we focus on the case where the hole concentration $\delta = 12.5\%$.

III. NN INTERACTION

As the NN interaction is the most remarkable one except for the on-site interaction, we focus on the effects of NN interaction on the t' -Hubbard model in this section.

A. Numerical convergence

Before discussing the results in our work, we will demonstrate the convergence of DMRG results and details in fitting the DMRG data. For this purpose, we plot the results for

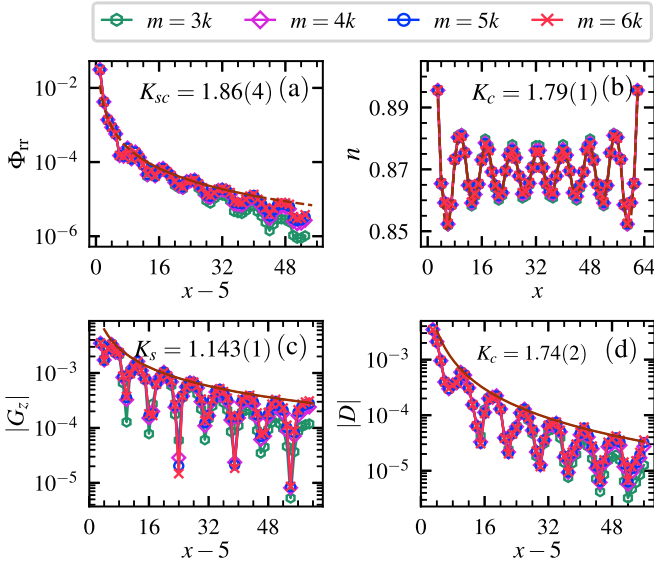


FIG. 2. DMRG results for $V = 0.4$ and $L = 64$. (a) shows the singlet pairing correlation function Φ_{tr} . Φ_{tr} is fitted by the function $B_{sc}(x - x_0)^{-K_{sc}}$, which is shown by the brown line. (b) displays the real-space density profile. The brown wavy line is the fitting via the function (3). (c) and (d) are the spin and charge density correlation, respectively. The brown lines are power-law fittings of top points with the formula $B_s(x - x_0)^{-K_s}$ and $B_c(x - x_0)^{-K_c}$, respectively. K_α ($\alpha = sc, s, c$) in the panel (a), (c), and (d) is the corresponding power exponent. The legend shows the states kept in the DMRG simulations where $k = 1000$.

$V = 0.4$ and $L = 64$ in Fig. 2 as a representative to show the convergence in pace with the number of retained states. For the future reference, we present some raw data of the ground-state energy in the Supplemental Material [55]. Here, we use the singlet pairing correlation to diagnose the superconductivity, which is defined as

$$\Phi_{\text{tr}}(x - x_0) = \langle \Delta_r^\dagger(x_0) \Delta_r(x) \rangle. \quad (2)$$

The spin-singlet pairing-field operator $\Delta_r^\dagger(x)$ is given by $\Delta_r^\dagger(x) = \frac{1}{\sqrt{2}} [c_{(x,0),\uparrow}^\dagger c_{(x,1),\downarrow}^\dagger - c_{(x,0),\downarrow}^\dagger c_{(x,1),\uparrow}^\dagger]$, where the site is labeled by (x, y) with the rung index x and leg index $y = 0, 1$. The subscript r means that the bond is along the rung direction. Similarly, we can define $\Delta_l^\dagger(x)$ with the bond along the leg direction. x_0 labels the reference position, which should be chosen carefully. First, it should be far enough from the edge to avoid the edge effect. Second, we should keep enough sites for a reliable fitting. In our calculations, we choose $x_0 = 5$ for $L = 64$ and $x_0 = 6$ for $L = 96$, respectively. We have checked that the fitted exponents are almost unchanged with a larger x_0 . The charge density profile is given by $n(x) = \langle n_{(x,0)} + n_{(x,1)} \rangle / 2$. z component of the spin correlation function is $G_z(x - x_0) = \langle S_{(x,y)}^z S_{(x_0,y)}^z \rangle$, and charge density correlation $D(x - x_0) = \langle n_{(x,y)} n_{(x_0,y)} \rangle - \langle n_{(x,y)} \rangle \langle n_{(x_0,y)} \rangle$. These two functions do not depend on the index y since the two legs are equivalent, which is confirmed numerically. The number of retained states m ranges from 3000–6000 with an increment of 1000. When the number is greater than or equal to 4000, all the results are well converged as shown in Fig. 2. Therefore,

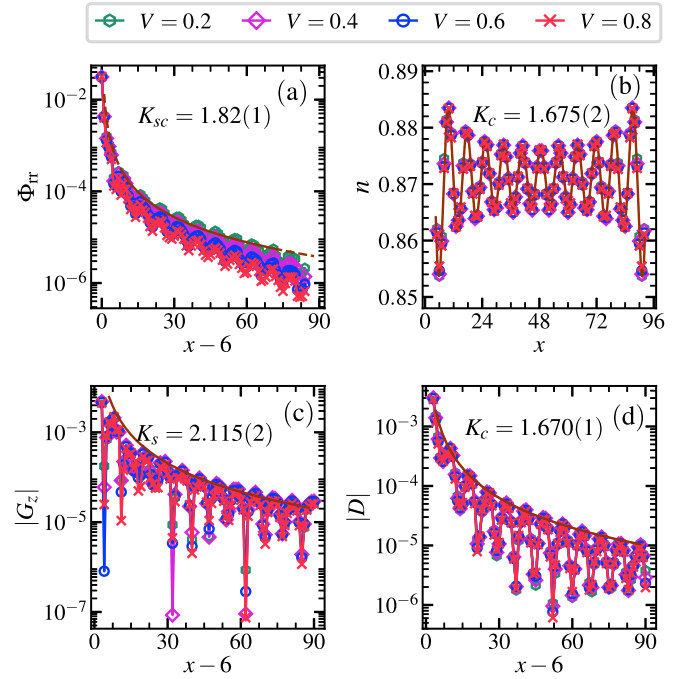


FIG. 3. The superconducting correlation, charge density profile, spin correlation, and density correlation are shown for repulsive NN interaction $V = 0.2, 0.4, 0.6,$ and 0.8 . The lattice size is $L = 96$. The brown lines in these figures are fittings of the results of $V = 0.2$, and the corresponding Luttinger parameter extracted is given in each panel.

in this case 4000 states are sufficient to obtain accurate numerical results.

We try to fit the superconducting correlation function Φ_{tr} by the power function $B(x - x_0)^{-K_{sc}}$, which is shown in brown line in Fig. 2(a). A good fitting suggests a superconducting ground state. The charge density distribution can be fitted via a trigonometric function multiplied by a spacing-dependent amplitude,

$$n(x) = n_0 + A \cos(Qx + \phi), \quad (3)$$

where $A = A_0 [x^{-K_c/2} + (L_x + 1 - x)^{-K_c/2}]$ and Q are the wave vector of CDW. The spin and density correlations behave in an oscillating form, so we use the top points to fit the correlations with a power function, which are shown in Figs. 2(c) and 2(d), respectively.

In addition, we also checked the convergence with respect to system sizes. For two sizes $L = 64$ and $L = 96$, the numerical results show that finite-size effects are negligible. Accordingly, for simplicity, we will use $L = 64$ or $L = 96$ to discuss our results.

B. Repulsive interaction

Now we consider the effects of the NN interaction V . And in this section we focus on the repulsive one, i.e., $V > 0$. Figure 3 shows the effects of the V on the superconducting correlation, charge density profile, spin correlation, and density correlation. The strengths of V ranges from 0.2–0.8 with an interval 0.2. First, we can see from Fig. 3(a) that as the V increases the superconducting correlation decreases. This

indicates that the superconducting correlation is weakened by the NN interaction. However, the power-law behavior is kept in the parameter range considered here and thus the V does not destroy the superconductivity. For the V as large as $V = 1.6$ (not shown here), the superconducting correlation still satisfies a power law. Second, $n(x)$, $G_z(x - x_0)$ and $D(x - x_0)$ are insensitive to V , which are shown in Figs. 3(b), 3(c), and 3(d). Figure 3(b) indicates that the CDW is robust in the presence of the NN interaction. The wavelength of charge density is $\lambda_c = 8$, and there is one hole in each stripe. In particular, $G_z(x - x_0)$ and $D(x - x_0)$ for $V = 0.2, 0.4, 0.6$, and 0.8 can be well fitted by a power function, respectively. Further, from the spin correlation function we can find domain walls in the antiferromagnetic background where holes are enriched. The period of spin order λ_s is about 16, which is twice of λ_c .

The numerical results above signify the robustness of the overall ground-state properties of the t' -Hubbard ladder against the repulsive NN interaction V . It is clear that the CDW and superconductivity coexist in the ground state. The NN repulsion weakens the superconducting correlation, but less impacts on the charge density distribution. When the NN interaction is small, the Luttinger parameter K_c extracted from the charge density function $D(x - x_0)$ is comparable to K_{sc} , as we show in Fig. 2. With the increase of repulsive NN interaction, we have $K_c < K_{sc}$. Namely, the CDW dominates in the ground state. These numerical results imply that the CDW is favorable in the presence of the NN repulsion.

C. Attractive interaction

The numerical results above indicate that the ground state is not inclined to superconductivity in the presence of repulsive NN interactions. Recent experiments on a one-dimensional cuprate chain can be well understood via the Hubbard model with an attractive NN interaction [47]. Furthermore, numerical simulations have identified an effective, attractive interaction induced in the one-dimensional Holstein-Hubbard model with long-range electron-phonon interaction [48]. The experimental and numerical works renewed the interest in the Hubbard model with attractive NN interaction [56–60]. In the one-dimensional chain, the ground state exhibits p -wave superconductivity [57]. And the correlation of d -wave superconductivity is enhanced by attractive interaction on a four-leg cylinder [58]. Here, we consider the t' -Hubbard model with attractive NN interaction on the two-leg ladder. Through extensive numerical simulations, we give more attention into how the superconducting correlation, density correlation, spin correlation, and single-particle correlation G_c are affected by the attractive NN interaction. Cooperating with recent numerical simulations, we can better understand the Hubbard model with attractive interaction.

The main results of attractive NN interaction are summarized in Figs. 4 and 5. In Fig. 4, the correlation functions on the two sides of $|V| = 0.60(5)$ have different dependencies on the NN attraction. When $|V| > 1.45(5)$, as shown in Fig. 5(d), the charge undulation in the bulk disappears and the system exhibits regions with enriched holes and electrons. According to these, a rough ground-state phase diagram can be mapped

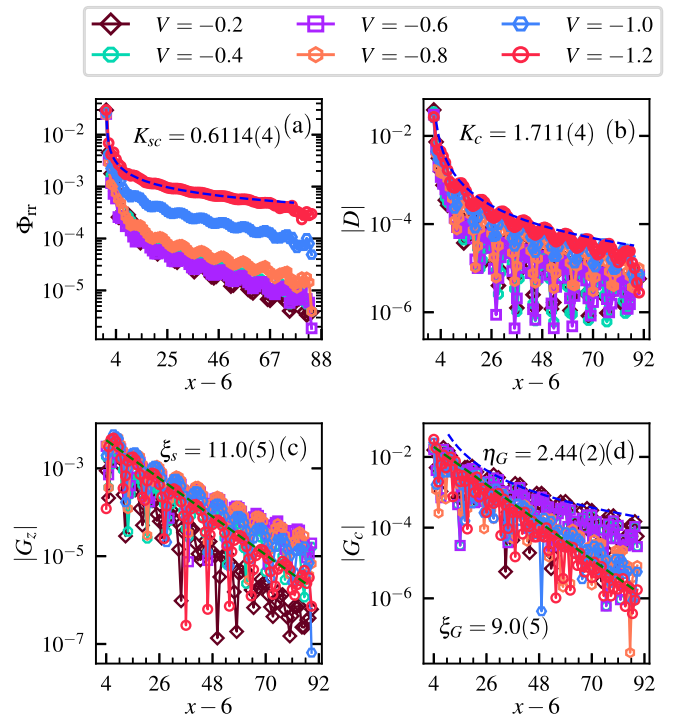


FIG. 4. Correlation functions for various attractive NN interactions. The lattice size is fixed $L = 96$. (a) is the superconducting correlation, and it increases with the increase of $|V|$. The enhancement of superconductivity becomes remarkable when $|V| > 0.8$. The density correlation function in (b) always decays algebraically. Though weak attraction slightly weakens the density correlation, it is strengthened by strong NN attraction. In (c), the spin correlation is enhanced under a small $|V|$ but it is suppressed by a large $|V|$, which corresponds to the closing and reopening of the spin gap. The single-particle Green function G_c , shown in (d), decays algebraically under a small $|V|$, but exhibits an exponential decay as V becomes strong, which implies that the single-particle excitation gap opens when strong attractive $|V|$ is introduced. ξ_α ($\alpha = s, G$) in (c) and (d) is extracted by fitting the correlation functions via $A_\alpha e^{-\frac{x-x_0}{\xi_\alpha}}$, and η_G in (d) is given by fitting the data at $V = -0.2$ via the formula $B_G(x - x_0)^{-\eta_G}$.

out. The ground state is a superconducting phase when $|V| < 0.60(5)$, it is an LE liquid phase for $0.60(5) < |V| < 1.45(5)$, and a PS when $|V| > 1.45(5)$.

In the superconducting phase, both the superconducting correlation and charge density correlation decay algebraically. Moreover, we found that $K_{sc} < K_c$. With the increase of $|V|$, the superconducting correlation is stable and only slightly enhanced while the density correlation and single-particle correlation is weakened marginally. In addition, the spin correlation decays exponentially and the single-particle correlation decays algebraically, implying gapped spin and gapless single-particle excitations. In this phase, as shown in Fig. 4(c), the spin correlation is enhanced when we increase $|V|$. After crossing the phase transition, the system is in an LE liquid superconducting phase, which is supported by the following evidence. First, K_{sc} and K_c satisfy the relation $K_{sc} \times K_c \sim 1$. The results of $|V| = 1.2$ is a prime example of this phase. The parameters K_{sc} and K_c , extracted from power fittings, are

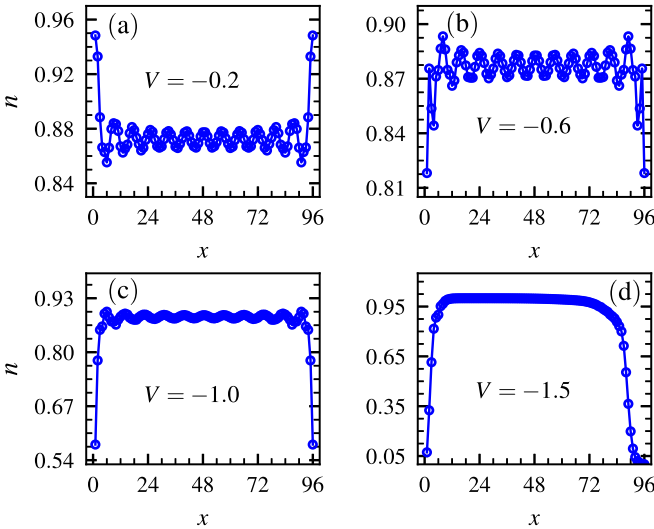


FIG. 5. Typical charge density distributions for different V with the system size $L = 96$. Since the open boundary condition is adopted, electrons prefer to stay at the boundaries for small $|V|$, while holes on the edges are energetically favorable for a large $|V|$. If V is not strong enough, as shown in (a), (b), and (c), the modulation of charge density is maintained. In (d), The modulation is destroyed by strong NN attractive interaction, electrons are gathered in bulk, and the holes are at the two edges, indicating a PS.

shown in Figs. 4(a) and 4(b), respectively, and their product gives 1.046. Second, in Fig. 4(c), the spin correlation shows an exponential decay when $|V|$ is far away from the critical point because of the reopen of a spin gap. The behavior of the single-particle Green's function shown in Fig. 4(d) has a noticeable change in comparison with that in the superconducting phase. It can be well fitted by an exponential function, thus the single-particle excitation is gapped. Due to finite-size effects, $K_{sc} \times K_c$ is larger than 1.0 when $|V|$ is much smaller than 1.2. The superconducting correlation, shown in Fig. 4(a), is significantly enhanced by the NN attraction. As the $|V|$ grows, the density correlation is also strengthened; at the same time, the valleys in density correlation become shallow. This is because that large $|V|$ tends to stabilize the CDW and thus the fluctuation becomes weak. From Figs. 4(c) and 4(d), it is clear that the spin and single-particle correlations are suppressed by $|V|$. Nevertheless, the superconductivity can not be continuously enhanced by the NN attraction. As shown in Fig. 5(d), the system is then driven into electron-hole phase separation by strong NN attraction. In this phase electrons and holes tend to occupy different regions. Due to the OBC employed in our DMRG simulation, the holes prefer to stay on the two edges while the electrons tend to stay in between, which is energetically favored when strong NN attraction is involved. Particularly, strong attraction destroys both the superconductivity and CDW. For example, when $|V| = 1.5$, as shown in Fig. 5(d), it is clear that the charge density distribution cannot be fitted by the function in Fig. 2. The evolution of the charge density distribution for various V is shown in Fig. 5.

Though the enhancement of superconducting correlation by NN attraction is analogous to the results of the four-leg cylinder [58], our results show that the t' -Hubbard model on

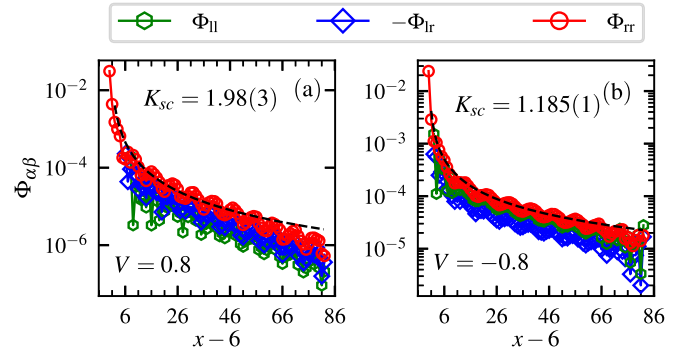


FIG. 6. Three different superconducting correlations, Φ_r , Φ_{rl} , and Φ_{ll} , for $L = 96$ are shown. Their behaviors in both cases tell us that d -wave superconductivity is favored.

a two-leg ladder with NN attraction displays some different behaviors from those on a four-leg cylinder. Here, we find $K_{sc} < K_c$ is always satisfied before entering PS phase, while this is satisfied on a four-leg cylinder only when $|V|$ is comparable to the NN hopping t . Moreover, though K_c increases when $|V| < 0.4(1)$ for the two-leg ladder, both K_c and K_{sc} decrease as $|V|$ increases in the range $0.4(1) < |V| < 1.45(5)$. This behavior is also distinct from that in a four-leg cylinder, where K_c and K_{sc} always have an opposite dependency on $|V|$. Before entering the PS, the superconducting correlation in Fig. 4(a) is enhanced overall by the NN attraction, while single-particle correlation is continuously weakened. Interestingly, the spin and density correlations shows an opposite nonmonotonic dependency on the NN attraction, which indicates that competition exists between them. Both the superconducting and density correlations decay algebraically, suggesting the coexistence of superconductivity and CDW in the superconducting and LE liquid phases, and superconducting dominates the ground state as $K_{sc} < K_c$.

D. Pairing symmetry

At the end of this section, we briefly discuss the pairing symmetry of the superconducting correlation. Though a two-leg ladder does not have the same spatial symmetry in the leg and rung direction, it may still help us to gain some insights into the pairing symmetry in the two-dimensional case. Here, three different superconductivity correlations, $\Phi_r(x - x_0)$, $\Phi_{rl}(x - x_0)$, and $\Phi_{ll}(x - x_0)$ are used to diagnose the pairing symmetry, where the index r and l indicate the bond in the rung and leg, respectively. The superconductivity correlations for two typical V are plotted in Fig. 6. The correlations between bonds in the same direction, i.e., Φ_r and Φ_{ll} , are positive, but Φ_{rl} is negative. This is the characteristic feature of the d -wave symmetry. Our results indicate that for the t' -Hubbard model, in the presence of repulsive or attractive NN interaction, the superconductivity tends to be d wave. When the strength of NN attractive interaction is comparable to NN hopping t , the d -wave superconductivity is significantly enhanced. The dependency of superconductivity on the NN attraction is consistent with recent DMRG simulations on a four-leg square cylinder [58]. Thus we expect that a d -wave

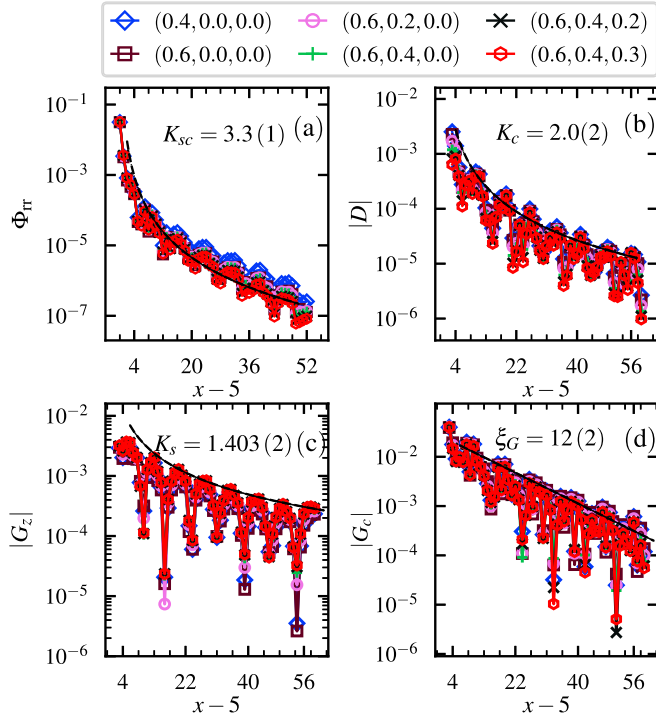


FIG. 7. Correlation functions with repulsive intersite interactions beyond the NN neighbor. The legends represent the values of intersite interaction in the form of (V_1, V_2, V_3) , which are shared by these subfigures. (a) is the superconducting correlation between rungs, the repulsive NNN interaction V_1 slightly weakens the correlation. For the third neighbor and the fourth neighbor interactions, the superconductivity correlations are nearly the same. Meanwhile, the superconductivity correlation is hard to be fitted by an exponential function, but a power function can give a good fitting. The spin correlation function, density-density correlation, and single-particle Green's function, shown in (b), (c), and (d), respectively, are insensitive to these interactions. Both the spin correlation and density correlation follow a power law. The single-particle Green function decays exponentially, and it satisfies $G_c(x-x_0) \sim e^{-(x-x_0)/\xi_G}$. The fittings in these subfigures are for $(0.6, 0.4, 0.2)$.

superconductivity may be stabilized by NN attraction in a two-dimensional square lattice.

IV. LONG-RANGE REPULSIVE INTERSITE INTERACTION

Now we consider the repulsive intersite interactions beyond the NN one, up to the fourth neighbors. In the following, we set the NN interaction $V = 0.8$. The results of $L = 64$ are shown in Fig. 7. The superconducting correlation is shown in Fig. 7(a). With the increase of the NNN interaction from $V_1 = 0.4$ to $V_1 = 0.6$, the superconducting correlation is suppressed slightly. However, with $V_1 = 0.6$ and the long-range third- and fourth-neighbor interactions involved, there is no remarkable effect on the superconducting correlation. The specific values of these interactions are given in the legend of Fig. 7 in the form of (V_1, V_2, V_3) . Just as in the case of NN interaction, the power law well fits the superconducting correlation, indicating the robustness of the superconductivity correlation to the long-range interactions. In the whole process, the

charge density profile (not shown), density correlation, spin correlation, and the single-particle Green's function are insensitive to these repulsive interactions. If we take a closer look, the density correlation and single-particle Green's function are subtly suppressed by these long-range interactions, while these long-range intersite interactions marginally enhance the spin correlation. Except that the single-particle Green's function decays exponentially, both spin and density correlations decay algebraically.

From the above numerical results, we can conclude that the ground-state properties of t' -Hubbard model are robust under these long-range repulsive intersite interactions. Though the intersite repulsion between electrons tends to weaken the superconductivity, the algebraic superconducting correlation is not destroyed by the intersite interactions. Since these repulsive intersite interactions always tend to weaken the superconductivity, reducing these repulsive interactions should be beneficial for the superconductivity.

V. VARIATION IN ON-SITE INTERACTION

In our discussion above, we fix the on-site interaction $U = 8$. In this section we turn to study the effects of on-site interaction. When electrons are less localized and the bandwidth are large, the U is relatively smaller. On the other hand, the physics of the large U limit of the Hubbard model under doping are also interesting. Here we take $V = \pm 0.4$ and consider several U . t and t' are fixed as before. Our results are shown in Fig. 8.

Despite some minor differences for $\pm|V|$, the charge density profile and the correlations in Fig. 8 share many common behaviors in their dependency on U . First, the superconducting correlation increases as U decreases and tends to be saturated. For example, the strength of the superconducting correlation at $U = 4$ is almost the same as that at $U = 2$. Second, the density distribution can be well fitted by the formula (3) only when U is around 8. For larger or smaller U , the CDW becomes unstable and the formula (3) is no longer valid. Moreover, the oscillation amplitude decreases and tend to disappear. Such an instability under a very large U agrees with a previous study of the Hubbard model on a four-leg cylinder [28]. Our results imply that uniform superconductivity is likely to form under a small U . Here, our numerical results demonstrate that there is no close relationship between the superconductivity and the stripe in the t' -Hubbard model on a two-leg ladder. The superconducting correlation is established at small U , and it is weakened as U increases. The power decay behavior is robust in the whole range of U considered here. However, the CDW appears only when $U_{c1} < U < U_{c2}$.

Under $\pm|V|$ interactions, the density-density correlations, spin correlations, and the single-particle Green's functions (not shown), obey a power-law decay behavior, implying that the spin excitation and charge excitation are gapless. The density correlations are slightly suppressed with the increase of U . Compared with the case of attractive V , the density-density correlation are easier to weaken under repulsive V . The spin correlation is enhanced at first and then suppressed when U increases, and it has a broader enhancement window for repulsive V .

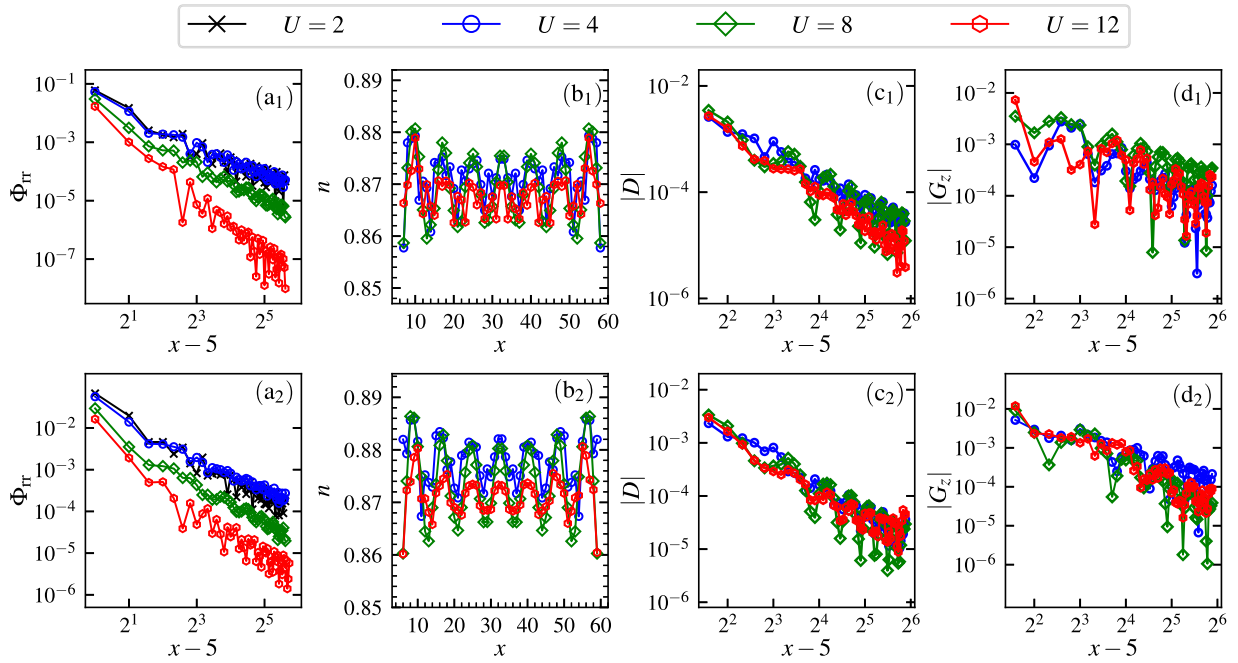


FIG. 8. With the system size $L = 64$, the two rows are the results under different Hubbard U for the NN interaction $V = 0.4$ and $V = -0.4$, respectively. From left to right, the columns are the superconducting correlation, charge density distribution, density correlation, and spin correlation. In (a₁) and (a₂), a large U tends to weaken the superconducting correlation. Under the same U , the superconducting correlation for a repulsive V is weaker than that for an attractive V . The CDW order, given in (b₁) and (b₂), is stable under medium strength of U , where $U = 6, 8, 10$. (c₁) and (c₂) display the density correlations. They decay algebraically and are slightly weakened overall with the increment of U . The spin correlations in (d₁) and (d₂) are enhanced at first and then suppressed as U increases. In both cases they decay in a power law. For clarity, except for the superconducting correlation of $U = 2$, the data for $U = 2, 6, 10$ are not shown.

VI. CONCLUSIONS

Using the DMRG method, we have systematically investigated how the intersite interactions affect the ground state of the t' -Hubbard model on a two-leg ladder. Our numerical results show that the repulsive intersite interactions do not change the ground state qualitatively, although such interactions do weaken the superconducting correlation qualitatively. On the other hand, when the NN interaction V is attractive both the spin and charge correlation functions become sensitive to such a interaction, and the superconducting correlation can be significantly enhanced. A strong enough NN attraction drives the system into a phase separation. Our numerical results give strong numerical evidence that the superconductivity is strengthened by a NN attraction, especially when V is comparable to the NN hopping amplitude t , agreeing with

a recent DMRG study on a four-leg cylinder. In addition, the charge density wave is favorable when U is around 8, both weaker and stronger U make the charge density unstable.

Our numerical results can help us understand the novel physics in superconducting cuprate ladder materials. Furthermore, since the ladder is a bridge between one- and two-dimensional systems, our work can also shed some lights in revealing the high- T_c superconductivity in cuprates.

ACKNOWLEDGMENTS

This work is supported by the National Key Research and Development Program of China (Grant No. 2022YFA1402704) and by the National Natural Science Foundation (Grants No. 12274187, No. 12047501, No. 12247101, No. 11834005).

- [1] B. Keimer, S. A. Kivelson, M. R. Norman, S. Uchida, and J. Zaanen, From quantum matter to high-temperature superconductivity in copper oxides, *Nature (London)* **518**, 179 (2015).
- [2] C. Proust and L. Taillefer, The remarkable underlying ground states of cuprate superconductors, *Annu. Rev. Condens. Matter Phys.* **10**, 409 (2019).
- [3] J. Hubbard, Electron correlations in narrow energy bands, *Proc. R. Soc. A* **276**, 238 (1963).
- [4] F. C. Zhang and T. M. Rice, Effective Hamiltonian for the superconducting Cu oxides, *Phys. Rev. B* **37**, 3759 (1988).
- [5] V. J. Emery, Theory of high- T_c superconductivity in oxides, *Phys. Rev. Lett.* **58**, 2794 (1987).
- [6] J. E. Hirsch and S. Tang, Antiferromagnetism in the two-dimensional Hubbard model, *Phys. Rev. Lett.* **62**, 591 (1989).
- [7] S. R. White, D. J. Scalapino, R. L. Sugar, E. Y. Loh, J. E. Gubernatis, and R. T. Scalettar, Numerical study of the two-dimensional Hubbard model, *Phys. Rev. B* **40**, 506 (1989).
- [8] M. Qin, H. Shi, and S. Zhang, Benchmark study of the two-dimensional Hubbard model with auxiliary-field quantum Monte Carlo method, *Phys. Rev. B* **94**, 085103 (2016).

- [9] A. Wietek, Y.-Y. He, S. R. White, A. Georges, and E. M. Stoudenmire, Stripes, antiferromagnetism, and the pseudogap in the doped Hubbard model at finite temperature, *Phys. Rev. X* **11**, 031007 (2021).
- [10] E. Gull, O. Parcollet, and A. J. Millis, Superconductivity and the pseudogap in the two-dimensional Hubbard model, *Phys. Rev. Lett.* **110**, 216405 (2013).
- [11] W. Wu, M. S. Scheurer, S. Chatterjee, S. Sachdev, A. Georges, and M. Ferrero, Pseudogap and fermi-surface topology in the two-dimensional Hubbard model, *Phys. Rev. X* **8**, 021048 (2018).
- [12] C. Hille, D. Rohe, C. Honerkamp, and S. Andergassen, Pseudogap opening in the two-dimensional Hubbard model: A functional renormalization group analysis, *Phys. Rev. Res.* **2**, 033068 (2020).
- [13] G. Ehlers, S. R. White, and R. M. Noack, Hybrid-space density matrix renormalization group study of the doped two-dimensional Hubbard model, *Phys. Rev. B* **95**, 125125 (2017).
- [14] M. Qin, C.-M. Chung, H. Shi, E. Vitali, C. Hubig, U. Schollwöck, S. R. White, and S. Zhang, Absence of superconductivity in the pure two-dimensional Hubbard model, *Phys. Rev. X* **10**, 031016 (2020).
- [15] Y. F. Kung, E. A. Nowadnick, C. J. Jia, S. Johnston, B. Moritz, R. T. Scalettar, and T. P. Devereaux, Doping evolution of spin and charge excitations in the Hubbard model, *Phys. Rev. B* **92**, 195108 (2015).
- [16] B.-X. Zheng, C.-M. Chung, P. Corboz, G. Ehlers, M.-P. Qin, R. M. Noack, H. Shi, S. R. White, S. Zhang, and G. K.-L. Chan, Stripe order in the underdoped region of the two-dimensional Hubbard model, *Science* **358**, 1155 (2017).
- [17] S. D. Edkins, A. Kostin, K. Fujita, A. P. Mackenzie, H. Eisaki, S. Uchida, S. Sachdev, M. J. Lawler, E.-A. Kim, J. C. S. Davis, and M. H. Hamidian, Magnetic field induced pair density wave state in the cuprate vortex halo, *Science* **364**, 976 (2019).
- [18] P. Corboz, S. R. White, G. Vidal, and M. Troyer, Stripes in the two-dimensional t - J model with infinite projected entangled-pair states, *Phys. Rev. B* **84**, 041108(R) (2011).
- [19] A. S. Darmawan, Y. Nomura, Y. Yamaji, and M. Imada, Stripe and superconducting order competing in the Hubbard model on a square lattice studied by a combined variational Monte Carlo and tensor network method, *Phys. Rev. B* **98**, 205132 (2018).
- [20] K. Ido, T. Ohgoe, and M. Imada, Competition among various charge-inhomogeneous states and d -wave superconducting state in Hubbard models on square lattices, *Phys. Rev. B* **97**, 045138 (2018).
- [21] T. I. Vanhala and P. Törmä, Dynamical mean-field theory study of stripe order and d -wave superconductivity in the two-dimensional Hubbard model, *Phys. Rev. B* **97**, 075112 (2018).
- [22] B. Ponsioen, S. S. Chung, and P. Corboz, Period 4 stripe in the extended two-dimensional Hubbard model, *Phys. Rev. B* **100**, 195141 (2019).
- [23] J. M. Tranquada, B. J. Sternlieb, J. D. Axe, Y. Nakamura, and S. Uchida, Evidence for stripe correlations of spins and holes in copper oxide superconductors, *Nature (London)* **375**, 561 (1995).
- [24] J. M. Tranquada, H. Woo, T. G. Perring, H. Goka, G. D. Gu, G. Xu, M. Fujita, and K. Yamada, Quantum magnetic excitations from stripes in copper oxide superconductors, *Nature (London)* **429**, 534 (2004).
- [25] Y. Kohsaka, C. Taylor, K. Fujita, A. Schmidt, C. Lupien, T. Hanaguri, M. Azuma, M. Takano, H. Eisaki, H. Takagi, S. Uchida, and J. C. Davis, An intrinsic bond-centered electronic glass with unidirectional domains in underdoped cuprates, *Science* **315**, 1380 (2007).
- [26] H.-C. Jiang and T. P. Devereaux, Superconductivity in the doped Hubbard model and its interplay with next-nearest hopping t' , *Science* **365**, 1424 (2019).
- [27] C.-M. Chung, M. Qin, S. Zhang, U. Schollwöck, and S. R. White (The Simons Collaboration on the Many-Electron Problem), Plaquette versus ordinary d -wave pairing in the t' -Hubbard model on a width-4 cylinder, *Phys. Rev. B* **102**, 041106(R) (2020).
- [28] Y.-F. Jiang, J. Zaanen, T. P. Devereaux, and H.-C. Jiang, Ground state phase diagram of the doped Hubbard model on the four-leg cylinder, *Phys. Rev. Res.* **2**, 033073 (2020).
- [29] X. Hao, C. Chia-Min, Q. Mingpu, U. Schollwöck, R. W. Steven, and S. Zhang, Coexistence of superconductivity with partially filled stripes in the Hubbard model, [arXiv:2303.08376](https://arxiv.org/abs/2303.08376).
- [30] M. Hirayama, Y. Yamaji, T. Misawa, and M. Imada, *Ab initio* effective Hamiltonians for cuprate superconductors, *Phys. Rev. B* **98**, 134501 (2018).
- [31] M. Hirayama, T. Misawa, T. Ohgoe, Y. Yamaji, and M. Imada, Effective Hamiltonian for cuprate superconductors derived from multiscale *ab initio* scheme with level renormalization, *Phys. Rev. B* **99**, 245155 (2019).
- [32] M. Uehara, T. Nagata, J. Akimitsu, H. Takahashi, N. Môri, and K. Kinoshita, Superconductivity in the ladder material $\text{Sr}_{0.4}\text{Ca}_{13.6}\text{Cu}_{24}\text{O}_{41.84}$, *J. Phys. Soc. Jpn.* **65**, 2764 (1996).
- [33] J. H. Schön, M. Dorget, F. C. Beuran, X. Z. Xu, E. Arushanov, M. Laguës, and C. D. Cavellin, Field-induced superconductivity in a spin-ladder cuprate, *Science* **293**, 2430 (2001).
- [34] N. Fujiwara, N. Môri, Y. Uwatoko, T. Matsumoto, N. Motoyama, and S. Uchida, Pressure-induced superconductivity in the spin-ladder cuprate, *J. Phys.: Condens. Matter* **17**, S929 (2005).
- [35] K. Kuroki, T. Kimura, and H. Aoki, Quantum Monte Carlo study of the pairing correlation in the Hubbard ladder, *Phys. Rev. B* **54**, R15641 (1996).
- [36] L. Balents and M. P. A. Fisher, Weak-coupling phase diagram of the two-chain Hubbard model, *Phys. Rev. B* **53**, 12133 (1996).
- [37] R. Noack, S. White, and D. Scalapino, The ground state of the two-leg Hubbard ladder a density-matrix renormalization group study, *Physica C: Superconductivity* **270**, 281 (1996).
- [38] S. Daul and D. J. Scalapino, Frustrated Hubbard ladders and superconductivity in κ -BEDT-TTF organic compounds, *Phys. Rev. B* **62**, 8658 (2000).
- [39] K. Louis, J. V. Alvarez, and C. Gros, Fermi surface renormalization in Hubbard ladders, *Phys. Rev. B* **64**, 113106 (2001).
- [40] G. B. Martins, J. C. Xavier, L. Arrachea, and E. Dagotto, Qualitative understanding of the sign of t' asymmetry in the extended $t - J$ model and relevance for pairing properties, *Phys. Rev. B* **64**, 180513(R) (2001).
- [41] M. Tsuchiizu and A. Furusaki, Generalized two-leg Hubbard ladder at half filling: Phase diagram and quantum criticalities, *Phys. Rev. B* **66**, 245106 (2002).
- [42] C. Degli Esposti Boschi, A. Montorsi, and M. Roncaglia, Brane parity orders in the insulating state of Hubbard ladders, *Phys. Rev. B* **94**, 085119 (2016).

- [43] A. Nocera, Y. Wang, N. D. Patel, G. Alvarez, T. A. Maier, E. Dagotto, and S. Johnston, Doping evolution of charge and spin excitations in two-leg Hubbard ladders: Comparing DMRG and FLEX results, *Phys. Rev. B* **97**, 195156 (2018).
- [44] L. F. Tocchio, F. Becca, and A. Montorsi, Superconductivity in the Hubbard model: A hidden-order diagnostics from the Luther-Emery phase on ladders, *SciPost Phys.* **6**, 018 (2019).
- [45] H.-C. Jiang, S. Chen, and Z.-Y. Weng, Critical role of the sign structure in the doped Mott insulator: Luther-Emery versus Fermi-liquid-like state in quasi-one-dimensional ladders, *Phys. Rev. B* **102**, 104512 (2020).
- [46] Y. Gannot, Y.-F. Jiang, and S. A. Kivelson, Hubbard ladders at small U revisited, *Phys. Rev. B* **102**, 115136 (2020).
- [47] Z. Chen, Y. Wang, S. N. Rebec, T. Jia, M. Hashimoto, D. Lu, B. Moritz, R. G. Moore, T. P. Devereaux, and Z.-X. Shen, Anomalous strong near-neighbor attraction in doped 1D cuprate chains, *Science* **373**, 1235 (2021).
- [48] Y. Wang, Z. Chen, T. Shi, B. Moritz, Z.-X. Shen, and T. P. Devereaux, Phonon-mediated long-range attractive interaction in one-dimensional cuprates, *Phys. Rev. Lett.* **127**, 197003 (2021).
- [49] S. R. White, Density matrix formulation for quantum renormalization groups, *Phys. Rev. Lett.* **69**, 2863 (1992).
- [50] S. R. White, Density-matrix algorithms for quantum renormalization groups, *Phys. Rev. B* **48**, 10345 (1993).
- [51] U. Schollwöck, The density-matrix renormalization group, *Rev. Mod. Phys.* **77**, 259 (2005).
- [52] U. Schollwöck, The density-matrix renormalization group in the age of matrix product states, *Ann. Phys. (NY)* **326**, 96 (2011).
- [53] A. Luther and V. J. Emery, Backward scattering in the one-dimensional electron gas, *Phys. Rev. Lett.* **33**, 589 (1974).
- [54] M. Fishman, S. R. White, and E. M. Stoudenmire, The itensor software library for tensor network calculations, *SciPost Phys. Codebases*, 4 (2022).
- [55] See Supplemental Material at <http://link.aps.org/supplemental/10.1103/PhysRevB.108.195136> for the ground-state energy.
- [56] M. Jiang, Enhancing d -wave superconductivity with nearest-neighbor attraction in the extended Hubbard model, *Phys. Rev. B* **105**, 024510 (2022).
- [57] D.-W. Qu, B.-B. Chen, H.-C. Jiang, Y. Wang, and W. Li, Spin-triplet pairing induced by near-neighbor attraction in the extended Hubbard model for cuprate chain, *Commun. Phys.* **5**, 257 (2022).
- [58] C. Peng, Y. Wang, J. Wen, Y. S. Lee, T. P. Devereaux, and H.-C. Jiang, Enhanced superconductivity by near-neighbor attraction in the doped extended Hubbard model, *Phys. Rev. B* **107**, L201102 (2023).
- [59] T. Tang, B. Moritz, C. Peng, Z.-X. Shen, and T. P. Devereaux, Traces of electron-phonon coupling in one-dimensional cuprates, *Nature Commun.* **14**, 3129 (2023).
- [60] H.-X. Wang, Y.-M. Wu, Y.-F. Jiang, and H. Yao, Spectral properties of 1D extended Hubbard model from bosonization and time-dependent variational principle: applications to 1D cuprate, [arXiv:2211.02031](https://arxiv.org/abs/2211.02031).